Scattering, Accommodation, and Trapping of HCl in Collisions with a Hydroxylated Self-Assembled Monolayer

James R. Lohr, B. Scott Day, and John R. Morris*

Department of Chemistry, Virginia Tech, Blacksburg, Virginia 24061

Received: April 5, 2005; In Final Form: June 1, 2005

Time-of-flight molecular beam scattering techniques are used to explore the energy exchange, thermal accommodation, and residence time of HCl in collisions with an OH-terminated self-assembled monolayer. The monolayer, consisting of 16-mercapto-1-hexadecanol ($HS(CH_2)_{16}OH$) self-assembled on gold, provides a well-characterized surface containing hydroxyl groups located at the gas−solid interface. Upon colliding with the hydroxylated surface, the gas-phase HCl is found to follow one of three pathways: direct impulsive scattering, thermal accommodation followed by prompt desorption, and temporary trapping through HO---HCl hydrogen bond formation. For an incident energy of 85 kJ/mol, the HCl transfers the majority, >80%, of its translational energy to the surface. The extensive energy exchange facilitates thermalization, leading to very large accommodation probabilities on the surface. Under the experimental conditions used in this work, over 75% of the HCl approaches thermal equilibrium with the surface before desorption and, for a 6 kJ/mol HCl beam, nearly 100% of the molecules that recoil from the surface can be described by a thermal distribution at the temperature of the surface. For the molecules that reach thermal equilibrium with the surface prior to desorption, a significant fraction appear to form hydrogen bonds with surface hydroxyl groups. The adsorption energy, determined by measuring the HCl residence time as a function of surface temperature, is 24 ± 2 kJ/mol.

1. Introduction

The chemical interactions of HCl on the surfaces of ice particles and liquid aerosols play a significant role in stratospheric and tropospheric chemistry. Although HCl is relatively inert in the gas phase, heterogeneous reactions in the stratosphere can convert these molecules into Cl_2, which, upon absorbing a photon, readily dissociate into ozone-destroying radicals. In the lower regions of the atmosphere, reactions between HCl and water or soot particles participate in atmospheric chemistry. Hydroxyl sites on the various surfaces can help sequester gas-phase reactants through hydrogen-bonding interactions, initiate a reaction by accepting a proton from HCl, or serve as a surface-bound reagent for hydrolysis or other reactions. Each of these processes is mediated by an initial gas−surface collision where the subsequent fate of an HCl molecule depends on the dynamics of the interaction. Our objective is to probe the nature of HCl surface collisions to help build a fundamental understanding of energy exchange, accommodation, and trapping when HCl collides with surface hydroxyl groups. The studies are facilitated by molecular beam techniques to control the HCl incident energy and OH-terminated self-assembled monolayers (SAMs) to provide a well-characterized surface containing isolated hydroxyl groups located precisely at the interface.

The dynamics of HCl−surface collisions involving hydroxylated systems have been explored by recent experimental and theoretical studies. Molecular beam scattering experiments have provided direct insight into the scattering, trapping, and protonation channels that accompany HCl (or DCl) collisions on liquid sulfuric acid[1,2] and glycerol.[3−5] The experiments reveal high trapping probabilities for the HCl (or DCl) in most systems. Of the number of DCl molecules trapped on a surface of glycerol, approximately 20% desorb back into the gas phase before reaction, 73% diffuse deeply into the liquid as ions, and 7% are found to undergo a rapid near-interfacial proton exchange reaction.[3] Theoretical simulations of HCl impinging on glycerol have shown that thermalization occurs on fast, 5 ps, time scales and that translational-to-HCl vibrational energy transfer does not occur even for 24 kcal/mol collisions.[5]

In addition to studies on liquids, numerous other groups have focused on the behavior of HCl at the surface of water ice. Recent simulations, often together with insightful experimental measurements, provide valuable information about the dynamics of hydrogen bond formation and subsequent dissociation of HCl at the surface of ice.[6−16] These studies reveal that the initial interaction occurs when HCl binds to a dangling H_2O oxygen atom via an H_2O---HCl hydrogen bond. Although a range of values have been calculated for the energy of the hydrogen bond, they are generally close to 20 kJ/mol for HCl bound to a single water molecule. Once trapped on a surface through hydrogen bond formation, the HCl molecules may dissociate if the chlorine atom is solvated by two adjacent dangling hydrogen atoms.[9] Alternatively, the HCl may diffuse molecularly below the first layer of water molecules where dissociation can occur by bulk solvation.[7] Computational results for HCl within water clusters demonstrate that dissociation can occur when HCl is embedded within a cluster of at least three water molecules.[17]

Additional experimental studies have also contributed to the understanding of HCl−water interactions. Molecular beam and temperature programmed desorption experiments have been applied to estimate the adsorption energy of molecular HCl on the surface of ice to be in the range of 25 kJ/mol to as high as 38 kJ/mol.[18−20] In addition, recent molecular beam scattering

* Address correspondence to this author. E-mail: morris@vt.edu.

10.1021/jp051733e CCC: $30.25
Published on Web 07/22/2005

experiments have been used to explore HCl thermalization and uptake on ice and HCl-doped ice films.[21] This work, in agreement with other investigations,[22] demonstrated that the thermal accommodation and uptake probabilities are very high for HCl on pure ice. The molecular beam studies also demonstrated that the residence time of HCl on pure ice can be extensive as HCl diffuses below the surface to become trapped within the bulk.[21]

Here, we report molecular beam scattering experiments of HCl on the surface of a hydroxyl-terminated self-assembled monolayer of alkanethiols on gold. The OH-terminated SAM provides the opportunity to study gas−surface energy exchange, thermal accommodation, and trapping on well-organized, atomically-flat systems where the interactions between HCl and OH groups are isolated at the interface. These experiments reveal three distinct scattering channels for HCl: impulsive scattering, thermal accommodation followed by prompt desorption, and trapping through the formation of hydrogen bonds.

2. Experimental Section

The SAMs used in this study were prepared by spontaneous chemisorption of 16-mercapto-1-hexadecanol ($HS(CH_2)_{16}OH$) from a 1 mM ethanolic solution onto a clean Au surface.[23] Below, we refer to the resulting hydroxyl-terminated monolayer as an OH-T SAM. The chemicals used in this study were purchased from Aldrich without further purification. The substrates were prepared by Au evaporation onto Cr-coated glass slides (EMF Corp.). The gold-coated glass slides were cleaned in a piranha solution (70/30 (v/v) mixture of H_2SO_4/H_2O_2) prior to use. The clean gold slides were placed in the solutions for at least 12 h, rinsed with copious amounts of ethanol, dried under a stream of ultrahigh purity nitrogen, and then immediately transferred to the main UHV chamber (base pressure $<5 \times 10^{-10}$ Torr) via a load-lock system. In the main chamber, the samples are mounted on a precision manipulator that is in thermal contact with a liquid nitrogen reservoir and a sample heater that provides control over the surface temperature from 155 to 500 K. The sample temperature is measured by a K-type thermocouple spot-welded adjacent to the monolayer surface samples. In addition, we have verified the surface temperature by recording the time-of-flight distributions for a pure atomic beam of Ar scattering from the surface. We find excellent fits to the final Ar TOF data using a Maxwell−Boltzmann distribution at the temperature of the surface as measured by the thermocouple. In measurements not shown here, reflection−absorption infrared spectra of the SAM in UHV (performed in our group) demonstrated that the 16-carbon OH-T SAM forms well-ordered, densely packed, and stable monolayers on the surface.[23]

The experimental setup is similar to molecular beam scattering systems described previously.[24−26] High-energy HCl beams are created by expanding 2% HCl in H_2 at 700 Torr through a 0.05 mm diameter nozzle (General Valve). After passing through a 0.40 mm diameter conical skimmer located 6 mm from the nozzle, the beam enters a differential pumping stage where it collides with a mechanical chopper wheel. The slotted wheel, rotating at 185 Hz, produces approximately 80 μs pulses of gas that then pass through a 1.5 mm collimating aperture and into a final differential pumping stage. The final pumping stage is separated from the main UHV chamber by a 2.2 mm aperture through which the beam passes to produce a 1 cm^2 spot size on the surface sample located in the main chamber, 36 cm from the nozzle. The peak energy of the 2% HCl in H_2 mixture is $E_i = 85$ kJ/mol, as measured by recording the time-of-flight distribution for a modulated beam directed at an in-line mass spectrometer. In addition, we have performed experiments with a low-energy HCl beam created by an expansion of 500 Torr of the pure gas through the nozzle. The energy of the pure HCl beam is estimated to be 6 kJ/mol.

The surface samples are aligned so that the normal is coplanar with the source and detector and at $\theta_i = 30°$ to the molecular beam. A fraction of the HCl that scatters from the surface is intercepted by a doubly differentially pumped Extrel mass spectrometer oriented at 60° to the incident beam such that $\theta_f = 30°$. The ionizer of the mass spectrometer is positioned 29 cm from the surface and views a 1 cm^2 spot size on the surface through two collimating apertures. The TOF distributions of the scattered HCl are determined by monitoring the mass spectrometer signal at m/z 36 as a function of time. Each TOF scan is initiated when a slit of the chopper wheel passes an LED-photodiode arrangement that sends a voltage pulse to trigger a multichannel scalar (Ortec). The multichannel scalar integrates signal from the spectrometer in 10 μs intervals. Electronic and timing offsets including trigger delays, ion flight times, and chopper-to-surface flight times are accounted for in analyzing the TOF spectra. [25,26]

The intensities and shapes of the TOF spectra were found to be highly stable and reproducible over the course of these studies. The stability in the experiments enables studies to be performed on surfaces at several different temperatures under identical conditions, facilitating direct comparisons of TOF spectra on relative scales. For each set of experiments presented below, where the data are plotted on a relative scale, we performed the measurements during the course of a 1-day period to minimize the effects of any slight changes in the beam intensity or mass spectrometer efficiency that may occur from day to day.

In addition to scattering studies, we also measured the uptake probability of HCl on the OH-T SAM at various surface temperatures. The uptake probability was determined, according to the King and Wells technique,[27] by measuring the differences in mass spectrometer signals for a blocked beam and when the beam collides directly with the surface sample. A reduction in signal is due to the net uptake of gas onto the SAM. However, we observed no net uptake of HCl at the surface temperatures used in this work. This result shows that HCl does not react significantly with the terminal groups or at the Au−S bond. Furthermore, XPS analysis of SAMs before and after prolonged HCl exposure revealed no changes in the elemental composition of the monolayer during the scattering experiments. These results are consistent with recent experiments that demonstrate extremely low reaction probabilities between alcohol molecules and HCl at the surface of ice.[28] Rather than reactions with the monolayer, the scattering pathways are determined by the dynamics of HCl energy exchange, thermal accommodation, and hydrogen bond formation with the outermost surface hydroxyl groups.

3. Results

3.1. Data Analysis. The scattering data are plots of the detector signal versus the flight time for molecules to traverse the distance between the surface and the ionizer of the mass spectrometer. The raw signal is proportional to number density $N(t)$ and is used to compute the probability $P(E_f)$ that an HCl molecule leaves the surface with final energy E_f. The translational energy distributions are computed from the relations $E_f = (1/2)m_{HCl}(L/t)^2$ and $P(E_f) \sim t^2N(t)$, where t is the HCl flight time.

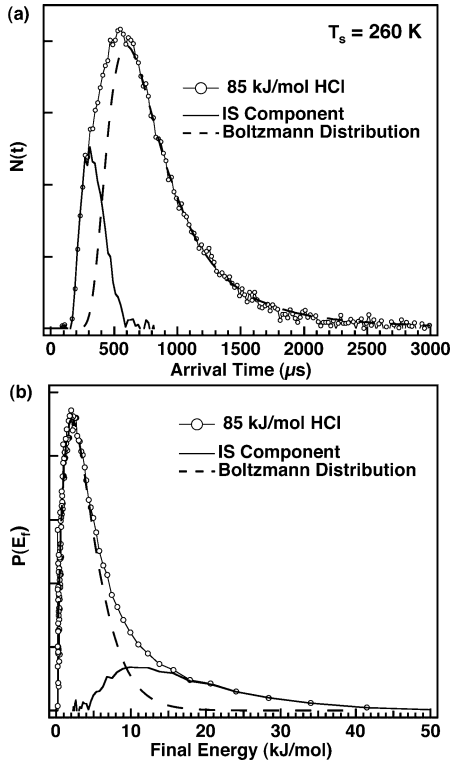

Figure 1. (a) A TOF spectrum, $N(t)$, for 85 kJ/mol HCl scattering from an $HS(CH_2)_{16}OH$ SAM on Au at a surface temperature of 260 K. (b) The corresponding final translational energy distribution $P(E_f)$ was derived from the TOF data in panel a. The dashed curves in each figure are Boltzmann distributions at 260 K, and the solid lines are the inelastic scattering components.

Figure 1a shows TOF data for the high-energy HCl beam scattering from the OH-terminated SAM. The high-velocity component of the data at early arrival times (~300 μs) is attributed to direct inelastic scattering. The component at later arrival times represents the molecules that have lost all, or the majority, of their excess energy to approach thermalization on the surface before recoiling back into the gas phase with a Boltzmann velocity distribution at the temperature of the surface.[29−35] The translational energy distribution, $P(E_f)$, in Figure 1b is separated into the direct inelastic scattering (IS) component and the Boltzmann component (BC) by assigning the BC to the part of the final energy distribution that falls within a Boltzmann distribution: $P_{BC}(E_f) = E_f(RT_s)^{-2} \exp(-E_f/RT_s)$. The Boltzmann distributions in Figures 1 (a) and (b) are represented by dashed curves. The inelastic component is assigned to the difference between $P(E_f)$ and $P_{BC}(E_f)$. As discussed below, the dynamics of gas−surface collisions are revealed through analysis of the fractional energy transfer to the surface in the inelastic channel, $(E_i - \langle E_{IS} \rangle)/E_i$, and the fraction of atoms that recoil (at $\theta_f = 30°$) with a thermal distribution of velocities (BC fraction). The BC fraction is defined as the weighting coefficient, α, in the relation $P(E_f) = \alpha P_{BC}(E_f) + (1 - \alpha)P_{IS}(E_f)$.[36]

3.2. High-Energy Scattering. Figure 1 shows that the fractional energy transfer in the impulsive scattering channel is extensive for the 85 kJ/mol beam incident on the OH-T SAM. Specifically, nearly all of the scattered HCl recoils from the surface with much less than 85 kJ/mol of translational energy. We find that, on average, over 80% of the HCl translational energy is transferred to the surface during the collision. The extensive energy exchange leads to significant thermalization on the surface. For the 85 kJ/mol beam incident at 30° to the surface normal, only 22% of the HCl molecules detected at the specular angle contribute to the impulsive scattering channel.

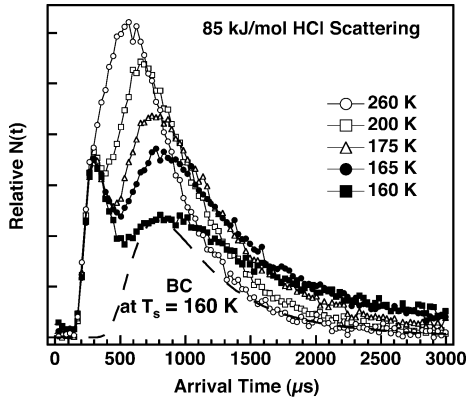

Figure 2. TOF spectra for 85 kJ/mol HCl scattering from the OH-T SAM at five different surface temperatures: 260, 200, 175, 165, and 160 K. The dashed curve represents a Boltzmann component (BC) at 160 K, scaled to fit the peak of the TOF data at that temperature. The failure of the Boltzmann distribution to fit the data is due to the finite residence time of HCl on the surface.

We have further explored the TOF characteristics for the impulsively scattered molecules by cooling the surface, which shifts the Boltzmann component to longer arrival times and isolates the impulsive channel. Figure 2 demonstrates that the intensity and overall shape of the impulsive component are independent of surface temperature. This result reveals that any changes in the OH-T SAM structure and density as the surface is cooled do not have a measurable influence on the energy exchange and overall thermalization probability. However, the dynamics of the molecules that thermally accommodate are greatly affected by surface temperature. As the surface is cooled, the thermal channel shifts to longer arrival times and is reduced in peak intensity. The broadening and shifting of this peak to longer arrival times is due, in part, to the lower energy Boltzmann component for thermal desorption from a lower temperature surface; however, a simple Boltzmann distribution fails to fit the long-time tail of the data for temperatures below about 200 K. For example, the dashed curve in Figure 2 represents a Boltzmann distribution for $T_s = 160$ K, the surface temperature at which the TOF data shown by the filled square symbols was recorded. The deviation from a simple thermal desorption description of the TOF data is attributed to the finite residence time of the HCl molecules on the surface.

The arrival time of a molecule in the TOF spectrum is described by:

$$t = t_{inc} + t_s + t_{scatt}$$

where t_{inc} and t_{scatt} are the flight times from the chopper to the surface and from the surface to the mass spectrometer, respectively, and t_s represents the surface residence time. As indicated above, the time for molecules to traverse the distance from the chopper to the surface, t_{inc}, is subtracted from the overall distribution during analysis, which means that the TOF distributions are sensitive to the surface-to-mass spectrometer flight times *and* the surface residence times. We have explored the residence time of HCl on the hydroxylated surface in detail by using a low-energy 6 kJ/mol HCl beam to minimize the contribution of impulsive scattering to the TOF distributions.

3.3. Low-Energy Scattering. As discussed below, surface temperatures lower than about 200 K yield three distinct scattering channels for the 85 kJ/mol HCl beam: (1) high-energy impulsive scattering, (2) prompt thermal desorption, and (3)

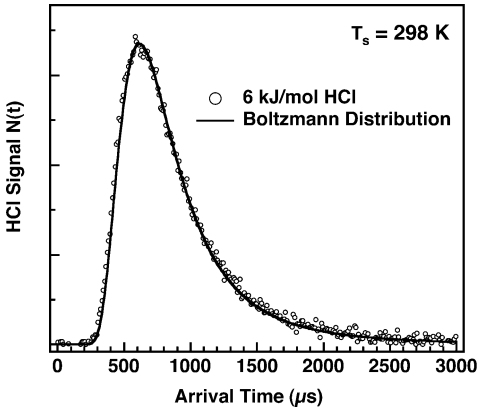

Figure 3. TOF distribution for 6 kJ/mol HCl scattering from the OH-T SAM with the surface held at 298 K. The solid line represents a Boltzmann component at this temperature. The good fit is evidence for near complete thermalization of the low-energy beam on the surface.

long-time desorption attributed to HCl hydrogen-bonding interactions with the surface OH groups. In an effort to isolate the two thermal components from the molecules that scatter impulsively, we employed a beam of HCl that has only 6 kJ/mol of incident energy. This beam completely or nearly completely thermally accommodates with the surface. Figure 3 shows that a Boltzmann distribution provides an excellent fit to the entire TOF data for 6 kJ/mol HCl scattering from the hydroxylated SAM at room temperature. However, as for the high-energy beam, we find that the finite residence time of the molecules on the surface results in the data deviating from a Boltzmann distribution at lower temperatures. Figure 4 shows TOF distributions for HCl scattering from a SAM at several different surface temperatures. The dotted curves that fit the early part of each data set are Boltzmann distributions at the temperature of the surface. The failure of the Boltzmann curve to describe the long-time tail to the data is due to the residence time.

For the low-energy beam, we can neglect impulsive scattering such that the entire TOF profile consists of a series of time-shifted Maxwell−Boltzmann distributions weighted by the probability, $p_{des}(t_s)$, that molecules in the incident gas pulse desorb from the surface at the time t_s:

$$N(t) = \int_0^t p_{des}(t_s) N_{MB}(t - t_s)\, dt_s$$

where N_{MB} is a Maxwell−Boltzmann distribution at the temperature of the surface and t_s is the residence time of the molecules on the surface.[1,3,37,38] We found that the TOF data are best described by a desorption probability function, $p_{des}(t_s)$, of the form:

$$p_{des}(t_s) = A \exp(-t_s/\tau_1) + B \exp(-t_s/\tau_2)$$

The parameters A and B and time constants τ_1 and τ_2 were found using a nonlinear least-squares procedure.[37] The desorption probability curves that provide the best fits to the $N(t)$ data (see Figure 4) are plotted in Figure 5. Figure 5 shows that as τ_2 increases (as required for fitting $N(t)$ at low temperatures), the long-time part of the desorption probability function, $p_{des}(t_s)$, increases in intensity. The increased probability for long residence times is reflected in Figure 4 as greater intensity in the $N(t)$ TOF distributions at long arrival times. Overall, we find that above a surface temperature of 200 K, we can fit the data well with a single exponential ($B = 0$) and a very short residence time, $\tau_1 < 20$ μs (this time is below the limit of our sensitivity to the surface residence time). For surface temperatures below about 200 K, the data are best described by a double exponential for $p_{des}(t_s)$ with short ($\tau_1 < 20$ μs) and long time constants differing by up to 2 orders of magnitude.

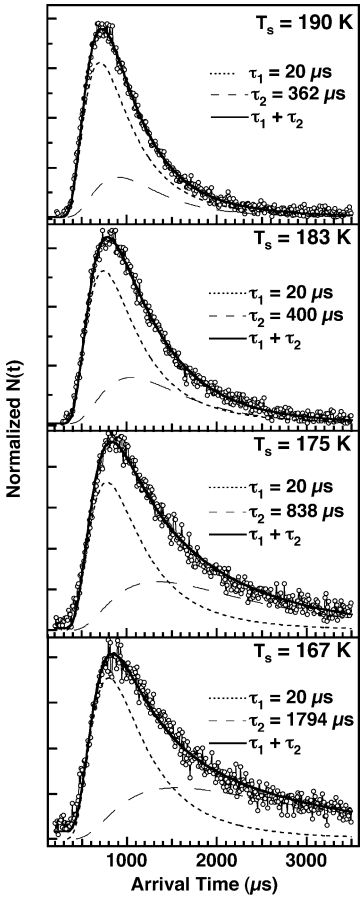

Figure 4. Four TOF distributions for 6 kJ/mol HCl scattering at different surface temperatures: 190, 183, 175, and 167 K. The solid curves that pass through the data points are calculated from a sum of time-shifted Boltzmann distributions that are weighted according to the desorption probability $p_{des}(t_s)$ as described in the text. The biexponential form of $p_{des}(t_s)$ is likely the result of two desorption channels. The prompt desorption channel is shown by the dotted curve and the delayed desorption channel is shown by the dashed curve in each panel.

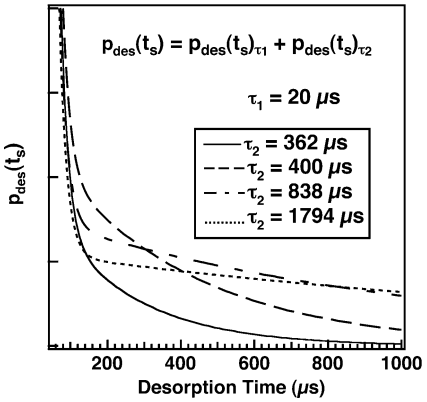

Figure 5. The time profiles for HCl desorption probability that provide the best fit to the TOF data presented in Figure 4. The best fits were obtained using a biexponential form for $p_{des}(t_s)$. Each exponential is characterized by a representative residence time, τ. The prompt desorption component is the same for each curve, $\tau_1 = 20$ μs (or anything below our experimental sensitivity of about 20 μs). The long-time component, τ_2, increases as the surface temperature decreases and ranges from 362 μs to 1794 μs.

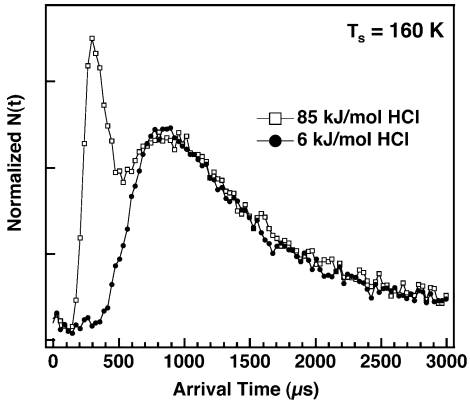

Figure 6. A comparison of the TOF distributions for scattering of the high-energy HCl beam and the low-energy beam. The spectra are normalized to the peak intensity of the thermal component to account for the differing fluxes of the two beams.

It should be noted that the relative intensities and residence times of the two thermal desorption channels are independent of incident translational energy. Figure 6 shows a direct comparison of the TOF distributions for high- and low-energy HCl beams scattering and desorbing from a surface at $T_s = 160$ K. We find that the only difference between the two profiles is the presence of impulsive scattering for the high-energy beam. The similarities in the thermal channels for the data of Figure 6 verify that once the molecules thermally equilibrate with the surface, they lose memory of their incident trajectory. The prompt thermal desorption channel in both high- and low-energy scattering is therefore most likely due to desorption of molecules that momentarily accommodate with the surface rather than due to molecules that scatter impulsively with a low final energy. Furthermore, since the incident kinetic energy does not influence the relative intensities of prompt and delayed desorption, ballistic penetration of the HCl into the SAM does not appear to contribute significantly to the dynamics. The data of Figure 6 also suggest that interactions between two adsorbed HCl molecules do not play a role in the scattering dynamics. This conclusion is based on the fact that the TOF distributions for the TD channel look identical for the high- and low-energy beam, despite the significant differences in the HCl fluxes for these two molecular beams. If adsorbate−adsorbate interactions were important, one would expect to observe evidence for these interactions by changing the coverage of adsorbates (or the flux of the incident gas). This conclusion is consistent with the estimated steady-state coverage of HCl on the surface, which is less than 10^{-4} ML, even for the longest residence time (coldest surface temperature) studied.

4. Discussion

Molecular beam scattering studies have been used to investigate the mechanisms of energy transfer, thermal accommodation, and adsorption in collisions of HCl with surface hydroxyl groups in an OH-terminated self-assembled monolayer. Our studies reveal that, as in many types of gas−surface collisions, energy transfer is extensive in the initial impact. In addition, we find that the majority of the molecules that are detected desorb from the surface in a thermal Maxwell−Boltzmann distribution at the temperature of the surface. For a low-energy HCl beam, nearly 100% of the molecules thermally accommodate with the surface before desorbing back into the gas phase. The efficient energy transfer and thermal accommodation may be facilitated by hydrogen-bonding interactions between the impinging molecules and the surface OH groups. In the sections below, we discuss our results to help develop an understanding of the HCl−OH interaction dynamics at the interface.

4.1. HCl Impulsive Energy Transfer. The TOF distributions for high-energy scattering shown in Figure 1 (a) reveal two distinct channels for HCl impinging on the 260 K surface. The long arrival time component is described well by a Boltzmann distribution at the temperature of the surface and represents the molecules that have fully dissipated their excess kinetic energy to accommodate with the surface. The second channel is evidenced by the signal recorded at early arrival times and represents those HCl molecules that recoil from the surface after an impulsive collision. Previous molecular beam studies and molecular dynamics simulations strongly suggest that, for our experimental arrangement, the impulsively scattered HCl molecules reach the detector most often after only a single collision with the surface.[39−41] The average energy for the impulsively scattered molecules is only about 10 kJ/mol, indicating that in a single-collision event, HCl transfers 88% of its impact energy to the surface.

The extensive energy exchange in the gas−surface collision is the result of very efficient coupling of the translational energy of the impinging molecule to isolated and concerted motions of the methylene chains within the monolayer. The SAM provides several degrees of freedom into which the translational energy of the impinging HCl molecules can be partitioned.[42] The concerted waving motions of the chains, vibrational modes along the chains, and hindered rotations of the OH groups can all be excited by the high-energy HCl. In addition, hydrogen bonds that exist between the surface hydroxyl groups[43,44] may serve as energy sinks during the collision as the impact disrupts the bonding network.[45] Finally, kinematic descriptions of gas−surface scattering predict extensive energy transfer for relatively massive particles colliding with light surface atoms,[30,46−48] which is the case for HCl colliding with the OH groups of the hydroxylated SAMs.

It is interesting to note that the energy transfer for HCl scattering from the OH-T SAM appears to be much more efficient than that observed in previous work for Ar scattering from OH-T SAMs.[24,49,50] The large variance may be due to a combination of factors that highlight the differences in molecular versus atomic scattering from a polar surface. In particular, HCl possesses internal degrees of freedom that may participate in the energy exchange event. However, previous work clearly demonstrates that HCl vibrations are rarely excited in gas−surface collisions at energies around 80 kJ/mol.[5] Therefore, the main differences in Ar and HCl scattering may be due to rotations of the scattered HCl and differences in the gas−surface potential energy landscape. Dipole−dipole forces may be strong enough in these systems to significantly affect the scattering dynamics. Future work in our group will focus on addressing these issues.

4.2. Thermal Accommodation and Adsorption. Along with extensive energy transfer in the initial gas−surface collision, HCl readily thermally accommodates on the hydroxylated surface. Specifically, for the 85 kJ/mol beam incident at 30° to the surface normal, 78% of the HCl molecules detected at the specular angle desorb from the surface in a thermal distribution. The extensive trapping may be facilitated by HO---HCl hydrogen-bonding interactions. Previous studies estimate the hydrogen-bonding energy of HCl to a single water molecule to be in the range of 19−25 kJ/mol.[9,17,51−53] The data presented in Figures 4 and 5 reveal the effect of these forces in regulating the desorption time of HCl from the hydroxylated SAMs. The fits

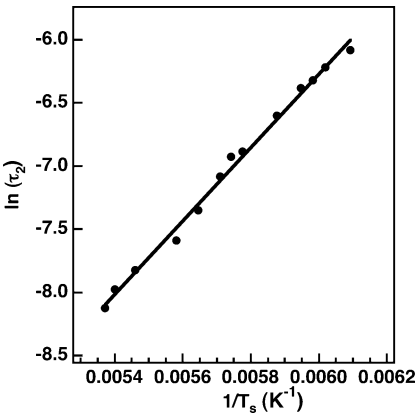

Figure 7. An Arrhenius plot of ln(τ_2) versus $1/T_s$. The gradient yields the apparent activation energy while the intercept provides the preexponential factor for the rate of desorption (see the text).

to the data in Figure 4 show that we are able to describe the final TOF distributions by using a double exponential form to model the residence time of the molecules on the surface.

The biexponential desorption probability function suggests that at least two separate channels govern the dynamics of the thermally accommodated molecules.[54] At warmer temperatures, the prompt desorption channel is the dominant component, while the slower component shifts to longer residence times and increases in intensity when the surface temperature is reduced. As described above, the delayed desorption channel is best described by a temperature-dependent characteristic residence time that varies over 2 orders of magnitude. We speculate that the long residence time channel for HCl represents the molecules that have diffused to a surface site and into an orientation that favors the formation of hydrogen bonds with the surface hydroxyl groups. The HCl molecules that do not find a favorable geometry for bond formation, before they desorb from the surface, contribute to the prompt thermal desorption channel.

4.3. Activation Energy. For a first-order desorption model, the time constants, τ_1 and τ_2, represent the characteristic residence times for molecules on the surface. The time constants are related to the surface temperature, T_s, and the activation energy, E_a, through:

$$\tau_i = \tau_o \exp(E_a/RT_s)$$

The first order rate constant is simply the inverse of this equation:

$$k = \nu \exp(-E_a/RT_s)$$

where $\nu = \tau_o^{-1}$ is the preexponential frequency factor.

Although the very short residence time ($\tau_1 < 20$ μs) of the prompt desorption pathway precludes our ability to determine the kinetic parameters for this channel, we are able to derive the values of E_a and τ_o for the slow component to desorption. Figure 7 shows an Arrhenius plot of ln(τ_2) versus $1/T_s$ developed by fitting numerous TOF distributions, collected at various surface temperatures, to the model described above. We find nearly identical results with the 6 kJ/mol and the 85 kJ/mol beams, but have focused here on the low-energy beam because the presence of the impulsive channel in the TOF distributions for high-energy scattering obscures the prompt desorption component and makes reliable nonlinear least-squares fitting difficult to achieve. The slope and intercept of the Arrhenius plot yield $E_a = 24 \pm 2$ kJ/mol and $\tau_o = 5 \times 10^{-11\pm1}$ s.

The activation energy for HCl of $E_a = 24 \pm 2$ kJ/mol agrees well with the estimates for H_2O---HCl hydrogen-bonding energy of 19 kJ/mol, calculated by Svanberg et al.,[9] and 22 kJ/mol, calculated by Toubin et al.[7] Although these calculations were performed for HCl bonding to ice surfaces, they provide some insight into the likely dynamics of HCl on the OH-terminated self-assembled monolayer studied here. The simulations on ice reveal that the initial HCl−surface bonding occurs through the formation of a single H_2O---HCl hydrogen bond formed when HCl diffuses to a dangling (free) oxygen atom on H_2O. In addition, spectroscopic measurements, in conjunction with computational studies, revealed that molecular HCl can hydrogen bond to dangling oxygen atoms on the surface of water clusters and small water−ice crystals.[15]

The dynamics of HCl on the hydroxylated SAM may be similar to the dynamics of HCl interacting with the topmost layer of OH groups on the surface of water ice. Simulations of OH-T SAMs have revealed a structure where the terminal groups form an extended −OH---OH hydrogen-bonding network that appears to leave one free hydrogen-bond acceptor site for each hydroxyl group.[44,55] Thermally accommodated HCl molecules that orient into a favorable geometry for hydrogen-bond formation can become trapped for extended residence times through 24 kJ/mol hydrogen-bonding interactions. However, hydrogen-bond formation appears to compete with desorption. The HCl molecules that do not hydrogen bond with the surface hydroxyl groups, before they are propelled back into the gas phase by the thermal motions of the surface atoms, contribute to the prompt desorption channel.

Although the measured desorption energy of 24 kJ/mol is consistent with a single hydrogen bond at the surface, the preexponential factor of $\tau_o = 5 \times 10^{-11\pm1}$ s is much greater than that expected for the first-order desorption of a small molecule from a surface. A "typical" preexponential factor, based on transition state theory, is approximately 10^{-13} s. The large prefactor suggests that desorption occurs through a lower entropy (more constrained) transition state. The recent work by Vogt and co-workers shows similar preexponential factors for the desorption of small alcohol molecules from the surface of an OH-terminated self-assembled monolayer.[56] Their temperature-programmed desorption studies indicated that surface diffusion into and subsequently out of the monolayer plays a significant role in the overall dynamics. Diffusion of surface-bound HCl molecules into the SAM may also contribute to the overall scattering dynamics in the work presented here. In addition, discontinuities in the ordered SAM caused by phase boundaries, missing rows, and single atom defects may play a role in the desorption dynamics.

Once the HCl molecules thermally equilibrate with the surface, it is reasonable to speculate that ionization can occur, resulting in a contact ion pair. In fact, previous studies show that HCl on the outermost surface of ice can dissociate if the Cl atom interacts with two adjacent dangling surface hydrogen atoms. In addition, recent calculations demonstrate that proton transfer from HCl to H_2O may be efficient enough to occur on very short time scales.[57] The specific surface interactions required for HCl dissociation/charge separation may also exist on the self-assembled monolayer surface. Further studies are needed to explore the role of proton transfer in the scattering dynamics of HCl on the well-ordered and atomically flat SAMs used in these investigations.

5. Summary

The dynamics governing collisions of HCl with surface hydroxyl groups have been explored using molecular beam

scattering techniques. The molecular beam provides control over the incident energy, while well-ordered self-assembled monolayers are used to afford a highly characterized surface with the hydroxyl groups isolated at the interface. Our studies reveal that energy transfer is extensive in the initial collision. Specifically, the HCl molecules that leave the surface after an impulsive collision at 85 kJ/mol retain only about 12% of their initial energy. In addition, nearly 78% of the molecules that we detect desorb from the surface in a thermal Maxwell−Boltzmann distribution at the temperature of the surface. For a low-energy HCl beam of 6 kJ/mol, we find that nearly 100% of the HCl molecules thermally accommodate with the surface before desorbing back into the gas phase.

The subsequent fate of thermally accommodated HCl molecules is regulated by the competition between immediate desorption and delayed desorption due to the formation of HO---HCl hydrogen bonds. At surface temperatures above about 200 K, the prompt desorption channel dominates the dynamics. However, as the surface temperature is decreased, the HCl appears to spend enough time on the surface to diffuse into a favorable geometry for hydrogen-bond formation, leading to an increase in delayed desorption from the surface.

Throughout the entire range of surface temperatures studied, we were able to describe the final time-of-flight distributions by weighting a series of time-shifted Boltzmann distributions with a double exponential desorption probability function that accounts for immediate and delayed desorption. The characteristic residence times used to model the delayed desorption channel have been used to construct an Arrhenius plot from which the preexponential factor and adsorption energy were determined. The adsorption energy of 24 ± 2 kJ/mol suggests that HCl is bound to this surface through a single HO---HCl hydrogen bond.

Acknowledgment. Funding for this work was provided by the National Science Foundation (CAREER Award No. CHE-94269). We would also like to thank Professors Gilbert M. Nathanson and Greg O. Sitz for helpful discussions.

References and Notes

(1) Morris, J. R.; Antman, M. D.; Nathanson, G. M. *J. Phys. Chem. A* **2000**, *104*, 6738.
(2) Behr, P.; Morris, J. R.; Antman, M. D.; Ringeisen, B. R.; Splan, J. R.; Nathanson, G. M. *Geophys. Res. Lett.* **2001**, *28*, 1961.
(3) Ringeisen, B. R.; Muenter, A. H.; Nathanson, G. M. *J. Phys. Chem. B* **2002**, *106*, 4999.
(4) Ringeisen, B. R.; Muenter, A. H.; Nathanson, G. M. *J. Phys. Chem. B* **2002**, *106*, 4988.
(5) Chorny, I.; Benjamin, I.; Nathanson, G. M. *JJ. Phys. Chem. B* **2004**, *108*, 995.
(6) Bolton, K. *J. Mol.Struct.* (*THEOCHEM*) **2003**, *632*, 145.
(7) Toubin, C.; Picaud, S.; Hoang, P. N. M.; Girardet, C.; Lynden-Bell, R. M.; Hynes, J. T. *J. Chem. Phys.* **2003**, *118*, 9814.
(8) Al-Halabi, A.; Kleyn, A. W.; Kroes, G. J. *J. Chem. Phys.* **2001**, *115*, 482.
(9) Svanberg, M.; Pettersson, J. B. C.; Bolton, K. *J. Phys. Chem. A* **2000**, *104*, 5787.
(10) Wang, L. C.; Clary, D. C. *J. Chem. Phys.* **1996**, *104*, 5663.
(11) Devlin, J. P.; Gulluru, D. B.; Buch, V. *J. Phys. Chem. B* **2005**, *109*, 3392.
(12) Buch, V.; Sadlej, J.; Aytemiz-Uras, N.; Devlin, J. P. *J. Phys. Chem. A* **2002**, *106*, 9374.
(13) Devlin, J. P.; Uras, N.; Sadlej, J.; Buch, V. *Nature* **2002**, *417*, 269.
(14) Uras, N.; Buch, V.; Devlin, J. P. *J. Phys. Chem. B* **2000**, *104*, 9203.
(15) Devlin, J. P.; Farnik, M.; Suhm, M. A.; Buch, V. *J. Phys. Chem. A* **2005**, *109*, 955.
(16) Farnik, M.; Weimann, M.; Suhm, M. A. *J. Chem. Phys.* **2003**, *118*, 10120.
(17) Re, S.; Osamura, Y.; Suzuki, Y.; Schaefer, H. F. *J. Chem. Phys.* **1998**, *109*, 973.
(18) Isakson, M. J.; Sitz, G. O. *J. Phys. Chem. A* **1999**, *103*, 2044.
(19) Graham, J. D.; Roberts, J. T. *J. Phys. Chem.* **1994**, *98*, 5974.
(20) Roberts, J. T. *Acc. Chem. Res.* **1998**, *31*, 415.
(21) Andersson, P. U.; Nagard, M. B.; Pettersson, J. B. C. *J. Phys. Chem. B* **2000**, *104*, 1596.
(22) Fluckiger, B.; Rossi, M. J. *J. Phys. Chem. A* **2003**, *107*, 4103.
(23) Nuzzo, R. G.; Dubois, L. H.; Allara, D. L. *J. Am. Chem. Soc.* **1990**, *112*, 558.
(24) Day, B. S.; Shuler, S. F.; Ducre, A.; Morris, J. R. *J. Chem. Phys.* **2003**, *119*, 8084.
(25) Ceyer, S. T.; Gladstone, D. J.; McGonigal, M.; Schulberg, M. T. *Molecular Beams*: *Probes of the Dynamics of Reactions on Surfaces*, 2nd ed.; Wiley: New York, 1988.
(26) Miller, D. R. *Atomic and Molecular Beam Methods*; Oxford University Press: New York, 1988; Vol. 1.
(27) King, D. A.; Wells, M. G. *Surf. Sci.* **1972**, *29*, 454.
(28) Graham, J. D.; Roberts, J. T. *Langmuir* **2000**, *16*, 3244.
(29) Barker, J. A.; Auerbach, D. J. *Surf. Sci. Rep.* **1984**, *4*, 1.
(30) Rettner, C. T.; Auerbach, D. J.; Tully, J. C.; Kleyn, A. W. *J. Phys. Chem.* **1996**, *100*, 13021.
(31) Harris, J. *Dynamics of Gas−Surface Interactions*; Royal Society of Chemistry: Cambridge, UK, 1991.
(32) Rettner, C. T.; Auerbach, D. J. *Science* **1994**, *263*, 365.
(33) Head-Gordon, M.; Tully, J. C.; Rettner, C. T.; Mullins, C. B.; Auerbach, D. J. *J. Chem. Phys.* **1991**, *94*, 1516.
(34) Rettner, C. T.; Schweizer, E. K.; Mullins, C. B. *J. Chem. Phys.* **1989**, *90*, 3800.
(35) Padowitz, D. F.; Peterlinz, K. A.; Sibener, S. J. *Langmuir* **1991**, *7*, 2566.
(36) Saecker, M. E.; Nathanson, G. M. *J. Chem. Phys.* **1993**, *99*, 7056.
(37) Brier, P. N.; Fletcher, J. N.; Gorry, P. A. *Surf. Sci.* **1996**, *365*, 525.
(38) Andersson, P. U.; Nagard, M. B.; Witt, G.; Pettersson, J. B. C. *J. Phys. Chem. A* **2004**, *108*, 4627.
(39) Day, B. S.; Morris, J. R. *J. Phys. Chem. B* **2003**, *107*, 7120.
(40) King, M. E.; Nathanson, G. M.; Hanning-Lee, M. A.; Minton, T. K. *Phys. Rev. Lett.* **1993**, *70*, 1026.
(41) M. E. King; Saecker, M. E.; Nathanson, G. M. *J. Chem. Phys.* **1994**, *101*, 2539.
(42) Cohen, S. R.; Naaman, R.; Sagiv, J. *Phys. Rev. Lett.* **1987**, *58*, 1208.
(43) Klein, H.; Battaglini, N.; Bellini, B.; Dumas, P. *Mater. Sci. Eng., C* **2002**, *19*, 279.
(44) Hautman, J.; Bareman, J. P.; Mar, W.; Klein, M. L. *J. Chem. Soc., Faraday Trans.* **1991**, *87*, 2031.
(45) Brewer, N. J.; Foster, T. T.; Leggett, G. J.; Alexander, M. R.; McAlpine, E. *J. Phys. Chem. B* **2004**, *108*, 4723.
(46) Tully, J. C. *J. Chem. Phys.* **1990**, *92*, 680.
(47) Grimmelmann, E. K.; Tully, J. C.; Cardillo, M. J. *J. Chem. Phys.* **1980**, *72*, 1039.
(48) Amirav, A.; Cardillo, M. J.; Trevor, P. L.; Lim, C.; Tully, J. C. *J. Chem. Phys.* **1987**, *87*, 1796.
(49) Day, B. S.; Davis, G. M.; Morris, J. R. *Anal. Chim. Acta* **2003**, *496*, 249.
(50) Shuler, S. F.; Davis, G. M.; Morris, J. R. *J. Chem. Phys.* **2002**, *116*, 9147.
(51) Mantz, Y. A.; Geiger, F. M.; Molina, L. T.; Molina, M. J.; Trout, B. L. *J. Phys. Chem. A* **2002**, *106*, 6972.
(52) Kisiel, Z.; Bialkowska-Jaworska, E.; Pszczolkowski, L.; Milet, A.; Struniewicz, C.; Moszynski, R.; Sadlej, J. *J. Chem. Phys.* **2000**, *112*, 5767.
(53) Xu, S. C. *J. Chem. Phys.* **1999**, *111*, 2242.
(54) Bond, P.; Prier, P. N.; Fletcher, J.; Jia, W. J.; Price, H.; Gorry, P. A. *Surf. Sci.* **1998**, *418*, 181.
(55) Sprik, M.; Delamarche, E.; Michel, B.; Rothlisberger, U.; Klein, M. L.; Wolf, H.; Ringsdorf, H. *Langmuir* **1994**, *10*, 4116.
(56) Vogt, A. D.; Beebe, T. P. *J. Phys. Chem. B* **1999**, *103*, 8482.
(57) Thompson, W. H.; Hynes, J. T. *J. Phys. Chem. A* **2001**, *105*, 2582.